Motion Recognition System of Table Tennis Players Based on MEMS Sensor

Wei Tang(✉) and Chonggao Chen

Huali College Guangdong University of Technology, Guangzhou 511325, China

Abstract. In order to improve the accuracy of table tennis players' movement recognition, a movement recognition system based on MEMS sensor is designed. The hardware part chooses MEMS sensor chip as the core processing chip, and designs the connection circuit of sensor. In the software part, the overlapped motion recognition signals are filtered, the network camera with certain parameters is used to obtain the motion parameters, and the recognition process is constructed. Simulation results show that the system has a high recognition accuracy of up to 99.9%, which has a certain application prospect.

Keywords: MEMS sensor · Table tennis player · Movement recognition · Noise data

1 Introduction

With the further development of computer graphics, computer vision and motion capture technology, the application of advanced optical motion capture system has far exceeded the early design. It can capture more detailed motion with more tracking points and higher speed. However, due to its limited camera coverage, complex tracking scheme and high price, it is difficult for ordinary users and small companies to use. For this reason, there are mechanical capture system, electromagnetic capture system and acoustic capture system.

The goal of motion recognition is to enable the robot vision system to see and distinguish different human movements like the human eye and brain, and complete the marking of unknown action types. Nowadays, it has been widely applied to the field of motion recognition of athletes. For example, someone has designed a real-time collection system of motion attitude data through the combination of FPGA and ARM, and designed a Kalman filter to eliminate the random noise in the collected data signal so as to achieve the detection of related movements [2]. Also, someone has studied the Dynamic Time Warping (DTW) algorithm, based on the spatial characteristic data collected from the basic technical movements of excellent table tennis players and young table tennis players of the national team, constructed a basic ball movement model of table tennis players of the national team by taking the loop ball with the backhand pull as an example, so as to analyze and identify the ball strokes of young table tennis players [3]. In order to accurately identify the movements of table tennis players and lay

W. Fu et al. (Eds.): ICMTEL 2021, LNICST 388, pp. 128–141, 2021.
https://doi.org/10.1007/978-3-030-82565-2_11

a good foundation for the next training and analysis, this paper studies the movement recognition system of table tennis players based on MEMS sensor. In the hardware part, MEMS sensor chip is selected as the core processing chip, and the sensor connection circuit is designed. In the software part, the overlapped motion recognition signals are filtered, and the motion parameters are obtained by using the network camera with certain parameters, and the recognition process is constructed, hoping to improve the table tennis players' action recognition level, and improve the table tennis players' action skills and efficiency.

2 Hardware Design of Athlete Movement Recognition System

2.1 Select MEMS Sensor Chip

The selection of the sensor chip determines the sampling rate of the high-speed sampling system. On the basis of satisfying the sampling rate of the system, the vertical resolution of the AD chip is also a parameter to be carefully considered, but the resolution is not directly proportional to the accuracy, and the high-resolution AD chip cannot provide high-precision sampling [4–6]. Because the sampling rate of this system reaches about ten MHz to thirty MHz, after comprehensive consideration, it is decided to adopt a AD9280 high-speed ADC chip provided by ADI Company. Its internal schematic diagram is shown in Fig. 1:

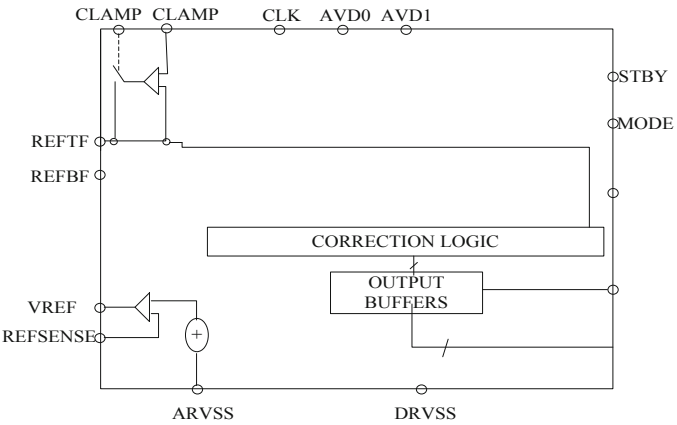

Fig. 1. Inner structure of sensor chip

The chip has a maximum sampling rate of 32 MSPS to support multiple sampling requirements, uses a vertical resolution of 8 bits, and combines bio-nano sensors. Single power supply is used to ensure low power consumption. Using its internal "embedded clamp" function, the integrated reference power supply circuit and sample and hold circuit. The error of differential nonlinearity (DNL) is controlled at 0.2 LSB, the IF subsampling is kept at 13 SMHZ, the reference voltage in the adjustable chip is used and the output mode of the three-state gate is adopted.

FPGA is a typical representative of programmable devices, which is based on PAL, GAL, CPLD and other programmable devices. Its level interface is quite rich, and it is easy to implement different kinds of protocols. In this system, the FPGA is required to complete the related logic control circuit functions, and at the same time to complete the task of storing a large number of collected data (the system intends to use SDRAM for data storage). Therefore, the choice of FPGA chip needs to include rich interface and logic resources, and can achieve the design requirements of SDRAM controller [7–9]. Therefore, after comprehensive consideration, it has been decided to adopt the EP4CE6F17C8 chip of Altera's Cyclone IV series as follows:

(1) It has as many as 6272 logical components/units, 392 LAB (Logic Macro Cell, programmable logical array)/CLB (Configurable Logic Block, configure logical modules), has very rich connection resources, and it runs very fast, up to 260 MHz.
(2) It is embedded with RAM up to 276480 bits, the main component of which is the M4K block of 4 KBit, and each block is very fast, up to 250 MHz. And configuration is flexible, each M4K module can be configured for a variety of memory, such as single-port or dual-port RAM, ROM and FIFO and so on.
(3) It has as many as 15 18 * 18 bit hardware multipliers built into it, runs at speeds up to several hundred MHz, and has selectable I/O registers.
(4) Two phase-locked loops (PLL) and 10 global clock networks shall be connected to facilitate the application and management of clock control. Provides a number of dedicated clock input pins.
(5) Capable of supporting multilevel single-ended I/O standards: 1.5 V, 1.8 V, 2.5 V and 3.3 V. High speed ports supporting various I/O standards, and providing up to 200 MHz DDR2 SDRAM interface, as well as 167 MHz QDRII SRAM and DDR SDRAM, this design uses these ports of FPGA to design SDRAM controller.

The system adopts HY57V2562GTR SDRAM chip, whose capacity is 256 Mbit, which can meet the requirements of the system, and its characteristics are: 256 Mbit (16M * 16 bit) storage capacity, 16blt bus. 8192 refresh cycle/64 ms. Power supply voltage, VDD = 3.3 V, VDDQ = 3.3 V. The 4M bit * 4banks* 16 I/O SDRAM functional module diagram is shown in Fig. 2:

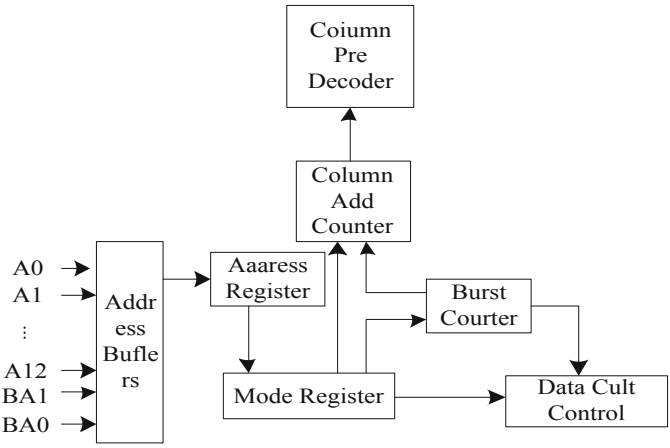

Fig. 2. Functional module diagram

As shown in Fig. 2, the hardware connection circuit is designed according to the functional module diagram shown in the diagram.

2.2 Design Hardware Connection Circuit

Under the control of the hardware card, there are many kinds of redundant resource outputs for the information of table tennis players, so when designing the hardware connection circuit, an output circuit is designed to realize the fault-tolerant function of hardware structure to data [10–12]. Set the voltage of the whole circuit to be between 3.3 V and 8 V. Set the resistance with low impedance and 10 Ω on the branch with few hardware components. Output a driving load at the same time. The output circuit is shown in Fig. 3.

Under the control of the output circuit structure shown in Fig. 3, the control processor in the control card is connected with pin 6, and the movement information of the table tennis player enters into the processing unit of the core through the pin 2. After being processed by the hardware core, the movement information is output through the pin 5. Control core processing board through the FGPA bus connection memory storage circuit, in the memory with the function of control, realize the external expansion of hardware circuit [13–15]. On the other side of the line bus, asynchronous serial interface is adopted, and the CPU processing board and the memory circuit are rationally arranged. Combined with RS422 standard four-wire system to regulate the movement data of athletes. Using the function of UART module integrated by processor and bridge chip, the level conversion form in circuit is set.

The hardware circuit of the system adopts an integral power module for power supply. Under the control of the storage circuit and the output circuit, the power supply demand of the hardware is divided into two parts. The first part supplies power to the integral hardware circuit, and the second part supplies power to the chip processor in the CPU board. A voltage converter is placed on the connecting line between the integral power supply and the hardware chip. In order to satisfy the stability between the hardware

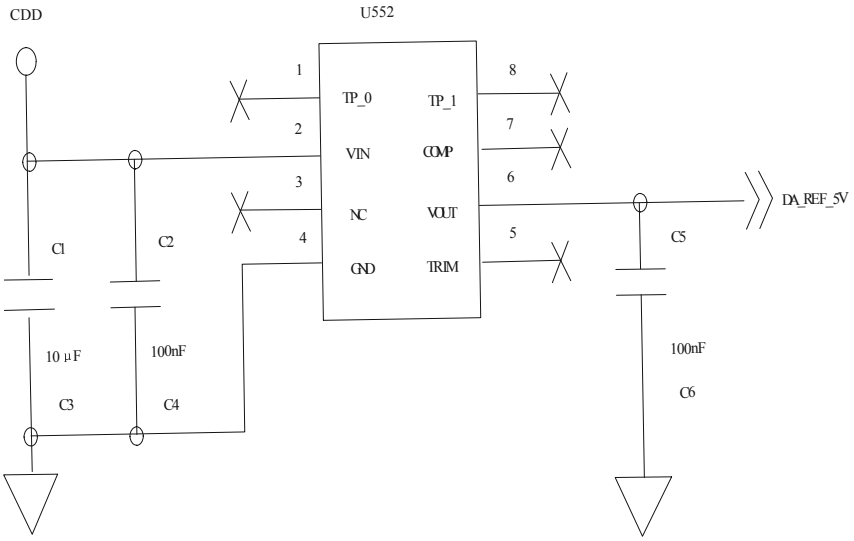

Fig. 3. Output circuit structure

components and the circuit, the voltage regulator is selected as the three-terminal voltage regulator of model AM S1084-3.3V [16–18].

3 Software Design of Athlete Movement Recognition System

3.1 Processing Overlapping Action Recognition Signals

The signals emitted by the single- chip microcomputer are generally in the form of a single channel. It is assumed that there are six commonly used digital modulation signals and noises in the time-frequency overlapping signals received by the single- chip microcomputer. The mathematical expressions are as follows:

$$r(t) = \sum_{i=1}^{6} s(t) + n(t) \tag{1}$$

Among them, $n(t)$ means Gaussian white noise, $s(t)$ means singlechip signal. The above generated overlapping signals are processed by sparse filtering with $n(t)$ numerically equal signals as overlapping signals, and the independent expression of overlapping signals can be recorded as shown in Fig. 2:

$$\begin{cases} s(t)_1 = \sum\limits_k \sqrt{E} a_k P(t - kT_e) \\ s(t)_2 = \sum\limits_k \sqrt{E}(a_k + jb_1) P(t - kT_e) \\ s(t)_3 = \sum\limits_k \sqrt{E} P(t - kT_e) f_0 \\ s(t)_4 = \sum\limits_k \sqrt{E} P(t - kT_e) \end{cases} \tag{2}$$

In formula (2), a_k represents the code element sequence, E signal energy, f_0 represents the initial phase of the carrier, T_e represents the code element width, and $P(t)$ represents the raised cosine pulse shaping function. According to the above sparse signal energy cumulants, the higher-order cyclic cumulants of the sum of several independent cyclostationary signals are equal to the sum of the higher-order cyclic cumulants of several signals. Assuming that the overlapping signals are independent, we can obtain:

$$C^a_{k,r}(\tau_1, \tau_1, ..., \tau_{k-1}) = \sum_{i=1}^{M} C^a_s + C^a_N \tag{3}$$

In formula (3), a denotes the cyclic frequency of the signal of the SCM, k denotes the cyclic cumulant, τ denotes the sparse filter parameter, and thus, if the cyclic frequency of several signals is known to be unequal and irreducible [19–21], the cyclic cumulant of several signals can be obtained respectively by calculating the cyclic cumulant of the received signals at different cyclic frequencies. Therefore, the feature parameters are set to highlight the difference of overlapping signal recognition. If the control delay parameter is 0, the first-order cyclic cumulant expression can be expressed as follows (4):

$$C^a_{r,10} = \frac{\sqrt{E}}{T_e} \int_{-\infty}^{\infty} P(t) dt \tag{4}$$

The characteristic parameters of the signals BPSK, QPSK, 8PSK and 16QAM are obtained by integrating the above overlapped signal characteristics using the formula of formula (4) first order cyclic cumulants as the calculation formula of the characteristic parameters. From the above analysis, it can be seen that only the first-order cyclic cumulants of 2FSK signals in the overlapped signals have values at the cyclic frequency, and the first-order cyclic cumulants of other signals are zero [22–25]. Therefore, the first order cyclic cumulants are used as the characteristic parameters to identify the 2FSK signals and the BPSK, QPSK, 8PSK and 16QAM signals. The feature is highlighted as a discrete spectral line on the frequency axis, and the 2FSK signal is identified by detecting the discrete spectral line. The signal selectivity of the cyclic cumulants results in the recognition process shown in Fig. 4:

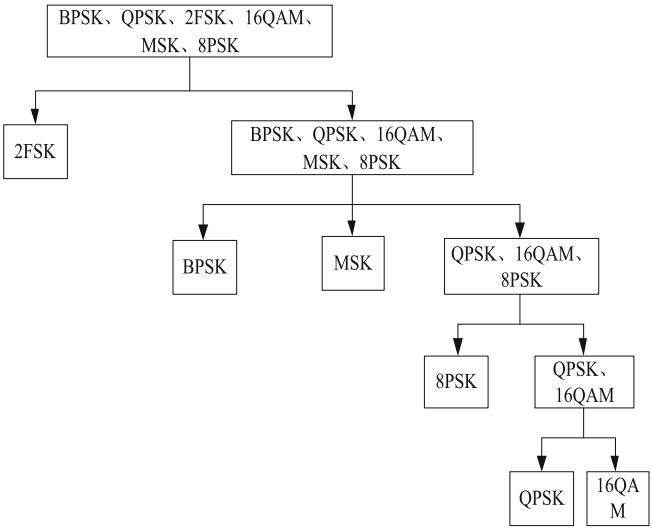

Fig. 4. Overlapping signal screening process

In the screening process shown in Fig. 4, in the background of Gaussian noise, the first order cyclic cumulant is used to eliminate the overlapping cumulant generated within the signal. After the overlapping signal is processed by sparse filtering, a software with recognition function is designed to finally complete the design of the motion recognition system.

3.2 Implementation of Software Action Recognition

In the application of motion recognition in real scene, it is necessary to use visual sensors to collect visual information. In view of the development trend of simple equipment and low cost in robot vision in the future [26–28], the TMV T828 (MINI) network camera, which is widely used at present, is selected to collect the imaging information of the actual scene, and its parameters are: USB2.0 interface, CMOS photosensitivity, and image imaging resolution 2048 $\times$ 1536. Based on the T828 (MINI) webcam, the application software system firstly utilizes the VideoCapture class in the OpenCV library as the video capture module to obtain the video equipment [29–31], and initializes the relevant parameters and sets the video object. The implementation process can be expressed as follows:

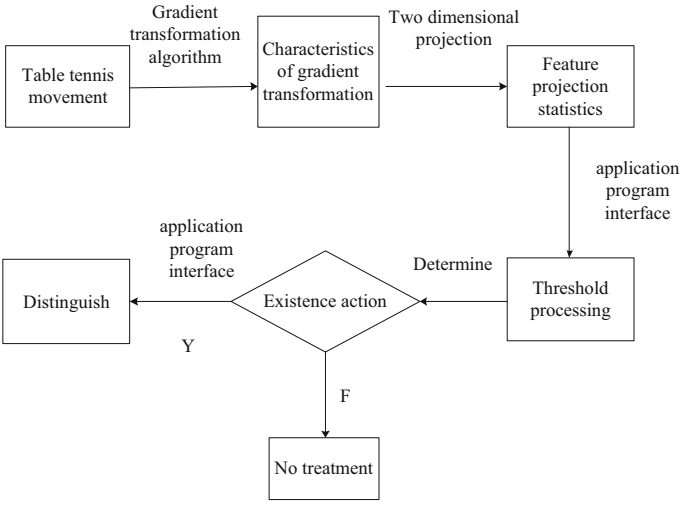

Fig. 5. Action recognition process

Under the realization flow shown in Fig. 5, the design of motion recognition system is finally realized.

4 Simulation Experiment

4.1 Construction of Development Environment

According to the non- functional requirements of the overall design of the identification system, the system uses ARM9 as the processor and reasonable peripheral hardware equipment, chooses Wince as the operating system of energy consumption acquisition software, and describes the structure of the action data acquisition system by modules according to the process.

Leads to 4 TTL serial port, 10 PIN JTAG interface and so on. GPRS interface module is used to transfer data to the server, RS485 and RS232 interface is used to collect data, NANDFLSAH is used to store energy consumption data, JTAG interface is used to debug hardware devices and bootloader burning. To take full advantage of the 2440's support for SD card startup, the produced superboot and object files are placed into the SD card for easier and faster installation or operation of various embedded systems (Windows CE 6/Linux, etc.). The S3C2440 itself has a total of 4 serial ports UARTO, 1, 2, 3, of which UARTO and 1 are a five-wire functional serial port and the other two are three-wire serial ports. All of these are greatly convenient for the use of embedded software system development. System hardware devices are shown in Fig. 6:

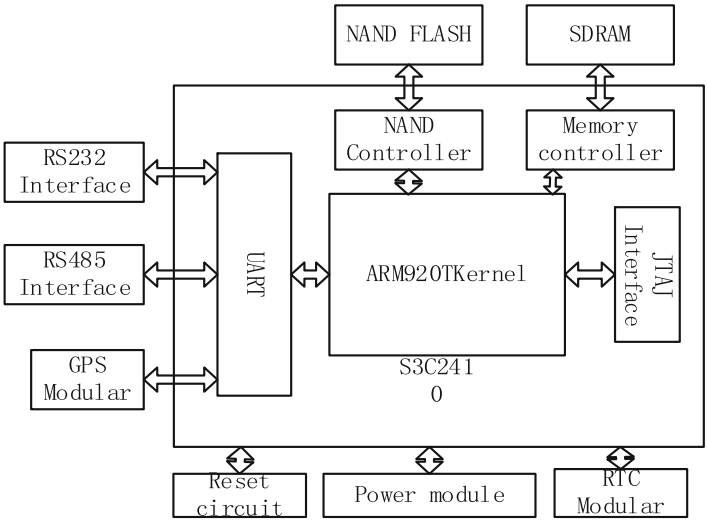

Fig. 6. Test environment

The data acquisition system takes S3C2410A as the processor, and communicates with the instrument through RS-485, RS-232 interface. When collecting RS-232 and RS-485 at the same time, the converter should be used. The converter can convert the single-ended RS-232 signal to the balanced differential RS-485 signal. The data is stored in NAND FLASH after the energy consumption equipment is collected, and finally the data is uploaded to the data center through the Ethernet interface. The real-time clock battery of the collector provides precise time for the equipment, and ensures the accuracy of the acquisition time (the real-time clock chip uses the crystal oscillator with high precision as the clock source). Insert the SD card into the card seat and use the SD card to flush the Wince operating system. Connect the LCD interface to the display screen, connect the 5 V power supply, and open the switch to start the operating system.

RS485 to TTL module metering equipment connected to the acquisition equipment, to achieve remote data communication with the measuring device. The controller communicates with the external measuring device through TTL serial port, sends instructions to the external measuring device, sets the relevant parameters of the external measuring device and collects the relevant measuring data. The serial port of TTL level is connected with the external measuring device through RS485/TTL converter to realize the mutual conversion of the standard serial interface. The RS485/TTL converter is compatible with the RS-232, RS-485 standard and can convert a single-ended RS-232 signal into a balanced differential RS-485 signal and transmit the collected data to the upper computer through the Ethernet interface. Set the pin description for the serial port, as shown in Table 1:

Table 1. Pin interface description

Pin	Definition	Explain			
		JTT-A-TTL	JTT-A-USB	JTT-A-232	JTT-A-485
1	GND	URAT input, TTL level	D−	Ground	A
2	RX/B/D−			Rx, 232 level	
3	TX/A/D+	URAT output, TTL level	D+	Tx, 232 level	B
4	VCC			DC5-7V	

After setting the pins, debug the serial port state and select the "Device Application" template. Then click the VS2008 menu tool "Connect to Device" and press F5 to start debugging. Finally, choose "Windows CE Devices" to start deployment, to this system after the completion of the hardware and software debug development environment setup. Then experiments are carried out by using the recognition system in document [2], document [3] and the recognition system designed in this paper to compare the performance of the three data acquisition systems.

4.2 Analysis of Experimental Results

Based on the above experimental preparation, 30 test users on the iPad are used as the load users of the identification system, and each five users are used as a test group to measure the response time results of the three action recognition systems under different number of user loads. The response time results are shown in Fig. 7:

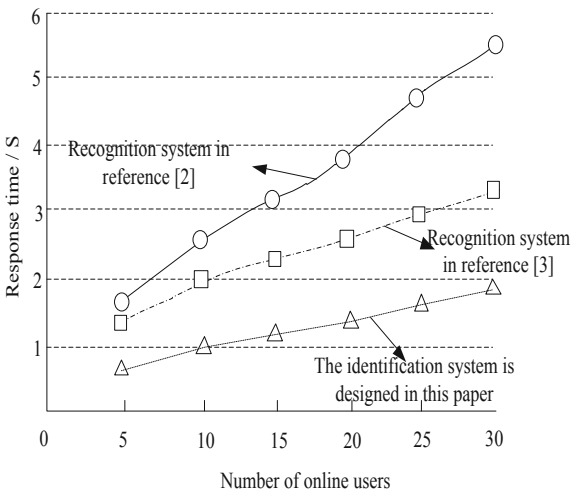

Fig. 7. Three identification system response times

The result of response time shown in Fig. 7 shows that the response time of the three identification systems gradually increases as the number of users accessing the action recognition system increases. When the number of online users is 30, the identification system in Document [2] has the longest response time and the final response time is about 5.5 s, and the identification system in Document [3] has the shortest response time. Under the control of the same number of online users, the final response time is about 3.3 s, while the identification system designed in this paper has the smallest response time and the value of response time is about 1.9 s. Compared with the above two identification systems, the final response time of the identification system designed in this paper is the shortest.

Keep the above experimental environment unchanged, select 10 of the 30 iPads used for the test, control the iPad to receive 50 identification resource data, when the visual image in the iPad is normal, test the number of packet loss, calculate and summarize the packet loss rate results. The packet loss rate results of the three identification systems are shown in Table 2:

Table 2. Results of packet loss rate of three identification systems

Test iPad serial number	Packet loss rate/%		
	Document [2] identification system	Document [3] identification system	Design system
1	0.78	0.50	0.15
2	0.75	0.47	0.19
3	0.74	0.45	0.18
4	0.74	0.47	0.23
5	0.73	0.49	0.17
6	0.80	0.45	0.25
7	0.79	0.48	0.24
8	0.78	0.49	0.18
9	0.77	0.46	0.21
10	0.78	0.50	0.21

Control three athletes' action recognition systems to recognize the same athletes' movements, count and calculate the packet loss rate. From the data in Table 2, we can see that the data of packet loss rate of the athletes' action recognition system used in Document [2] is the highest, the data of packet loss rate produced by each iPad is about 0.76%, the data of packet loss rate produced by the athletes' action recognition system used in Document [3] is less, the average packet loss rate is about 0.47%, and the data of packet loss rate produced by the recognition system designed in this paper is about 0.20. Compared with the above two resource recognition systems, the data of packet loss rate produced by the resource recognition system designed in this paper is the smallest, and

the movements received by athletes are more complete in the actual process of movement recognition.

Assuming that the categories of athlete movements to be identified in the three recognition systems are Categories 1, 2, 3, 4, 5 and 6, and 50 sets of movement information are prepared for each movement information type, if the identified identifiers are the same as the identifiers in the movement information, it is a successful recognition process. Under the control of the three movement recognition systems, the accuracy rates of movement recognition for different categories of athletes are calculated and counted as shown in Table 3:

Table 3. Accuracy results of three recognition systems

Categories of information	Accuracy of action recognition/%		
	Document [2] identification system	Document [3] identification system	Design system
Category 1	79.4	88.6	96.2
Category 2	76.6	89.1	99.9
Category 3	77.7	85.2	96.6
Category 4	76.1	85.6	98.6
Category 5	79.5	87.3	98.7
Category 6	78.2	89.7	96.6
Mean value	77.91	87.58	97.76

As can be seen from Table 3, the three recognition systems show different recognition accuracy for the same number and types of athletes, and the average accuracy of the above table can be seen, the recognition accuracy of the recognition system in [2] literature is about 77.91%, and the recognition accuracy is low. When the recognition system in document [3] is used in practice, the final recognition accuracy is about 87.58%, and the accuracy is high. The final recognition accuracy of the system is about 97.76%. Compared with the above two systems, the accuracy of the system is the largest and the recognition is the most accurate.

5 Concluding Remarks

Motion recognition is an important guarantee for the friendly interaction between robot and AI, and it is also a research hotspot in robot vision, AI and robot technology. In this paper, the problem of low accuracy in current motion recognition is analyzed, and a motion recognition system based on MEMS sensor is designed to recognize the motion of table tennis players accurately. The simulation results show that the shortest recognition response time of the system is about 1.9 s, the packet loss rate is about 0.20, and the recognition accuracy is up to 97.76%. However, due to time constraints, the system still has some shortcomings, which will be the focus of the next step.

References

1. Liu, S., Sun, G., Fu, W.: e-Learning, e-Education, and Online Training. Springer, Cham (2020). https://doi.org/10.1007/978-3-030-63955-6
2. Chen, J., Chen, H., Wang, J., et al.: Design of data acquisition and trajectory recognition system based on MEMS sensor. Chin. J. Electron Devices **42**(02), 463–468 (2019)
3. Feng, Z., Xiao, Y., Cao, Z., et al.: Rationality evaluation of young table tennis players' striking action based on DTW: taking the backhand topspin loop for example. J. Shanghai Univ. Sport **44**(06), 76–84 (2020)
4. Liu, S., Bai, W., Zeng, N., et al.: A fast fractal based compression for MRI images. IEEE Access **7**, 62412–62420 (2019)
5. Liu, S., Li, Z., Zhang, Y., et al.: Introduction of key problems in long-distance learning and training. Mob. Netw. Appl. **24**(1), 1–4 (2019)
6. Xie, G., Liu, Y., Lu, Y., et al.: Human behavior recognition based on time-domain features of MEMS inertial sensors. Piezoelectr. Acoustooptics **41**(02), 221–224 (2019)
7. Jun, J., Wang, X., Xu, Y., et al.: Study on a MEMS sensor with embedded state machines and its application in body position detecting. Chin. High Technol. Lett. **28**(03), 244–250 (2018)
8. Zhang, M., Huang, Y., Gao, Q., et al.: Brain plasticity of table tennis athletes based on dynamic amplitude of low-frequency fluctuation method. J. Shanghai Univ. Sport **44**(06), 62–69 (2020)
9. Li, B., Jin, P., Wu, Z., et al.: Design of ping-pong recognition based on S_Kohonen neural network. J. Huazhong Univ. Sci. Technol. (Nat. Sci. Ed.) **48**(03), 52–56 (2020)
10. Zhao, Y., Lan, Y., Qu, X.: Design of personnel positioning system in coal mine underground based on MEMS sensor. Ind. Mine Autom. **44**(08), 87–91 (2018)
11. Xie, G., Huang, X., Li, Y., et al.: Review of research on step detection algorithm with MEMS-based acceleration sensor. Appl. Res. Comput. **35**(12), 3526–3532 (2018)
12. Cui, J., Cao, H., Zhu, J., et al.: Human gait monitoring system based on MEMS tilt sensors and thin film pressure sensors. China Meas. Test. Technol. **44**(08), 70–75 (2018)
13. Yang, Y., Zhang, L., Qi, Y., et al.: Intravascular ultrasound image recognition based on residual network. Comput. Simul. **37**(04), 269–273 (2020)
14. Cem, D., O'Connor, N.E.: Temporal segmentation and recognition of team activities in sports. Mach. Vis. Appl. **29**(5), 891–913 (2018)
15. Li, Y.M., Li, B., Wang, X.X., et al.: Application of energy cost in evaluating energy expenditure in multi-ball practice with table tennis players. Zhongguo ying yong sheng li xue za zhi = Zhongguo yingyong shenglixue zazhi = Chin. J. Appl. Physiol. **35**(4), 331–335 (2019)
16. Zemková, E., Muyor, J.M., Jeleň, M.: Association of trunk rotational velocity with spine mobility and curvatures in para table tennis players. Int. J. Sports Med. **39**(14), 1055–1062 (2018)
17. Ukhov, I., Bjurgert, J., Auer, M., et al.: Online problem gambling: a comparison of casino players and sports bettors via predictive modeling using behavioral tracking data. J. Gambl. Stud. 1–21 (2020)
18. Yüksel, M.F., Sevindi, T.: Examination of performance levels of wheelchair basketball players playing in different leagues. Sports **6**(1), 18 (2018)
19. Zhou, Y., Chen, C.T., Muggleton, N.G.: The effects of visual training on sports skill in volleyball players - ScienceDirect. Progr. Brain Res. **253**, 201–227 (2020)
20. Heo, G., Ha, J.E.: Analysis of table tennis swing using action recognition. J. Inst. Control **21**(1), 40–45 (2015)
21. Xu, B., Ye, H., Zheng, Y., et al.: Dense dilated network for video action recognition. IEEE Trans. Image Process. **28**(10), 4941–4953 (2019)
22. Hu, G., Cui, B., Yu, S.: Joint learning in the spatio-temporal and frequency domains for skeleton-based action recognition. IEEE Trans. Multimedia **22**(9), 2207–2220 (2020)

23. Ryu, J.H., Seo, J.O., Jebelli, H., et al.: Automated action recognition using an accelerometer-embedded wristband-type activity tracker. J. Constr. Eng. Manag. **145**(1), 04018114.1–04018114.14 (2019)
24. Sun, Y.-H., Zhou, J.-Q., Zhang, X.-F.: Human motion pattern recognition based on acceleration sensor. Comput. Syst. Appl. **29**(06), 196–203 (2020)
25. Liu, D., Ji, Y., Ye, M., et al.: An improved attention-based spatiotemporal-stream model for action recognition in videos. IEEE Access (99), 1 (2020)
26. Chen, H., Liu, W., et al.: Fast retinomorphic event-driven representations for video gameplay and action recognition. IEEE Trans. Comput. Imaging **6**, 276–290 (2019)
27. Li, B., Jin, P., Wu, Z.: Design of ping-pong recognition based on S_Kohonen neural network. J. Huazhong Univ. Sci. Technol. (Nat. Sci.) 2020(3), 52–56 (2020)
28. Sun, X.: Research of human motion recognition based on long short-term memory. Wuxian Hulian Keji **164**(16), 23–24+41 (2019)
29. Li, X., Yang, J., Yang, J., et al.: Action recognition algorithm based on depth motion maps and regularized representation. J. Electron. Meas. Instrum. **32**(01), 119–128 (2018)
30. Sun, Y.-H., Zhou, J.-Q., Zhang, X.-F.: Human motion pattern recognition based on acceleration sensor. Comput. Syst. Appl. **29**(06), 196–203 (2020)
31. Liu, T., Li, Y., Liang, Z.: Human action recognition based on multi-perspective depth motion maps. J. Image Graph. **24**(03), 80–89 (2019)